October 2003

A Wideband, Synthetic Aperture Beamformer for Through-The-Wall Imaging

Fauzia Ahmad
Villanova University

Moeness G. Amin
Villanova University

Saleem A. Kassam
University of Pennsylvania, kassam@seas.upenn.edu

Gordon J. Frazer
Defence Science and Technology Organisation

Copyright 2003 IEEE. Reprinted from *IEEE International Symposium on Phased Array Systems and Technology 2003*, pages 187-192.
Publisher URL: http://ieeexplore.ieee.org/xpl/tocresult.jsp?isNumber=28113&page=2

A Wideband, Synthetic Aperture Beamformer for Through-The-Wall Imaging

Abstract

A coarray-based aperture synthesis scheme using subarrays and post-data acquisition beamforming is presented for through-the-wall wideband microwave imaging applications. Various effects of the presence of the wall, such as refraction, change in speed, and attenuation, are incorporated into the beamformer design. Simulation results verifying the proposed synthetic aperture technique for a TWI system are presented. The effects of incorrect estimates of the parameters of the wall, such as thickness and dielectric constant, on performance are investigated.

A WIDEBAND, SYNTHETIC APERTURE BEAMFORMER FOR THROUGH-THE-WALL IMAGING*

Fauzia Ahmad[1], Moeness G. Amin[1], Saleem A. Kassam[2], Gordon J. Frazer[3]

[1]Center for Advanced Communications, Villanova University, Villanova, PA 19085
E-mail: fahmad@ece.vill.edu; moeness@ece.vill.edu

[2]Moore School of Electrical Engineering, University of Pennsylvania, Philadelphia, PA 19104
E-mail: kassam@ee.upenn.edu

[3]ISR Division, DSTO, Edinburgh, Australia
E-mail: frazer@ieee.org

ABSTRACT

A coarray-based aperture synthesis scheme using subarrays and post-data acquisition beamforming is presented for through-the-wall wideband microwave imaging applications. Various effects of the presence of the wall, such as refraction, change in speed, and attenuation, are incorporated into the beamformer design. Simulation results verifying the proposed synthetic aperture technique for a TWI system are presented. The effects of incorrect estimates of the parameters of the wall, such as thickness and dielectric constant, on performance are investigated.

1.0 INTRODUCTION

"Seeing" through obstacles such as walls, doors, and other visually opaque materials, using microwave signals offers powerful tools for a variety of applications in both military and commercial paradigms. Through-the-wall imaging (TWI) can be used in rescue missions, behind-the-wall target detection, surveillance and reconnaissance. Existing and under development microwave TWI systems have been reviewed by Ferris and Currie [1]. Most of these systems can provide a range resolution of a few inches but have poor spatial resolution. In this paper, we use an aperture synthesis scheme based on the coarray formalism for improved spatial resolution. The coarray was originally defined for narrowband far-field active imaging [2], and is represented by a set of pair-wise sums of the position vectors of the elements in the transmit and receive apertures. The concept of coarrays was also extended to wideband imaging in [3].

The aperture synthesis technique using subarrays, was first proposed in [4] for ultrasound applications. In this scheme, the transmit and receive arrays are divided into subarray pairs, where each subarray consists of a single transmitter and one or more receivers. The subarrays are used independently to form component complex images of the scene by post-data acquisition beamforming [4]. These independent component images are then added coherently to obtain the composite complex amplitude image with the desired spatial resolution. This scheme was later generalized in [5] to incorporate subarrays composed of multiple transmitters using the concept of coarrays.

The subarray aperture synthesis scheme was recently extended to wideband microwave imaging, particularly for TWI applications [6,7]. Both these systems divide the transmit and receive arrays into single transmitter/single receiver subarray pairs. Although the work in [7] uses single transmitter/single receiver pairs, our work in [6] provides a general framework for array synthesis, and permits the realization of desired imaging characteristics by the use of the synthesized aperture. The analysis in [6] did not include a key factor of the problem, namely refraction due to the presence of the wall and the effect of inaccuracies in the wall parameters on TWI.

The composition and thickness of the wall, its dielectric constant, and the angle of incidence all affect the characteristics of the signal propagating through the wall [8]. The propagating wave slows down, encounters refraction, and is attenuated as it passes through the wall. In this paper, we present a microwave imaging system based on the concepts of subarrays and coarrays, whose design incorporates these effects. Post-data acquisition processing is used to implement the synthetic aperture beamformer for TWI.

In a practical situation, the wall parameters such as its thickness and dielectric constant, are not known apriori. Therefore, reasonable estimates of these parameters have to be used in beamforming. Any errors in estimating the wall parameters will compromise the beamformer design. An analysis of the effect of erroneous wall parameters on the performance of the beamformer is also provided.

* This work was supported by DARPA under Grant No. MDA972-02-1-0022. The content of the information does not necessarily reflect the position or the policy of the Government, and no official endorsement should be inferred.

0-7803-7827-X/03/$17.00 ©2003 IEEE.

The paper is organized as follows. Section 2 gives an overview of post-data acquisition beamforming in the absence of the wall. In Section 3, we present the design of the synthetic aperture beamformer for TWI. The performance of the proposed system is demonstrated through simulation results. Section 4 deals with the beamformer in the presence of erroneous estimates of wall parameters. Section 5 contains the concluding remarks.

2.0 POST-DATA ACQUISITION BEAMFORMING IN THE ABSENCE OF THE WALL

Consider an M-element transmit and an N-element receive line array, both located along the x-axis, which are divided into single transmitter/single receiver subarrays. The region to be imaged is located along the positive z-axis. Let the m-th transmitter, placed at location $\mathbf{x_{tm}}$, illuminate the scene with a wideband signal $s(t)$. The reflection by any target located in the region being imaged is measured and stored by the n-th receiver located at $\mathbf{x_{rn}}$. For a single point target located at $\mathbf{x_p}=(R_p\sin\theta_p, R_p\cos\theta_p)$, the output of the n-th receiver is given by $a(\mathbf{x_p})s(t-\tau_{mn})$, where $a(\mathbf{x_p})$ is the complex reflectivity of the target and τ_{mn} is the propagation delay encountered by the signal as it travels from the m-th transmitter to the target at $\mathbf{x_p}$, and back to the n-th receiver, as shown in Fig. 1. This delay is given by

$$\tau_{mn} = (d(\mathbf{x_{tm}}, \mathbf{x_p}) + d(\mathbf{x_p}, \mathbf{x_{rn}}))/c \tag{1}$$

where c is the speed of light and $d(\mathbf{x},\mathbf{y})$ denotes the Cartesian distance between locations $\mathbf{x}$ and $\mathbf{y}$. This process is repeated with the m-th transmitter, until all the N receivers have been used sequentially. The corresponding N outputs are processed as follows. The region of interest is divided into a finite number of pixels in range and angle. The complex composite signal corresponding to the image of the pixel located at $\mathbf{x_q}$, is obtained by applying time delays and weights to the N received signals, and summing them. The resulting output for a single target case is given by

$$z_{mq}(t) = \sum_{n=1}^{N} w_{rn} a(\mathbf{x_p}) s(t-\tau_{mn}-\tilde{\tau}_{mn}) \quad , \quad \tilde{\tau}_{mn} = (2R_q - d(\mathbf{x_{tm}}, \mathbf{x_p}) - d(\mathbf{x_p}, \mathbf{x_{rn}}))/c \tag{2}$$

where w_{rn} is the weight applied to the output of the n-th receiver, and $\tilde{\tau}_{mn}$ is the focusing delay applied to the output of the n-th receiver when the transmitter is at the m-th location. The focusing delay synchronizes the arrivals at different receivers for the same pixel, and thus allows coherent imaging of the scene. The above process is repeated by sequential use of the M transmitters and produces M complex composite signals, $z_{mq}(t)$, m=1,2,... M, corresponding to the image of the pixel at $\mathbf{x_q}$. The complex amplitude image value for the pixel located at $\mathbf{x_q}$ is obtained as

$$I(\mathbf{x_q}) = \left(\sum_{m=1}^{M} w_{tm} z_{mq}(t) \right)_{t=2R_q/c} \tag{3}$$

where w_{tm} is the weight applied to the component signal $z_{mq}(t)$ obtained using the m-th transmitter. The process, described by (2)-(3), is performed for all pixels in the region of interest to generate the composite image of the scene. The general case of multiple targets can be obtained by superposition.

3.0 DESIGN OF THE BEAMFORMER IN THE PRESENCE OF THE DIELECTRIC WALL

3.1 Refractions

Consider a wall of thickness d_w and dielectric constant ε. A signal traveling along θ_j through a wall-to-air interface will bend away from the normal on transmit (see Fig. 2). The angle of refraction θ_{jr} is given by Snell's law as

$$\theta_{jr} = \sin^{-1}(\sqrt{\varepsilon}\sin\theta_j) \tag{4}$$

Due to refraction, a signal traveling to the point $\mathbf{x_j} = (R_j\sin\theta_j, R_j\cos\theta_j)$ would instead travel to the point $\tilde{\mathbf{x}}_\mathbf{j} = (R_j\sin\tilde{\theta}_j, R_j\cos\tilde{\theta}_j)$. In order to develop the relationship between θ_j and $\tilde{\theta}_j$, we denote l_{j1} as the distance traveled by the signal through the wall along θ_j, and l_{j2} as the distance traveled, after refraction, to $\tilde{\mathbf{x}}_\mathbf{j}$. The parameters d_w, ε, R_j, θ_j, and θ_{jr} are all assumed to be known. The parameters l_{j1}, l_{j2}, and $\tilde{\theta}_j$ are all unknown. From Fig. 2, we obtain

$$l_{j1} = d_w/\cos\theta_j \tag{5}$$

Applying the cosine law to the triangle with vertices (**0**, **A**, $\tilde{\mathbf{x}}_\mathbf{j}$) and solving for l_{j2}, we get

$$l_{j2} = \sqrt{R_j^2 - l_{j1}^2\sin^2(\theta_j-\theta_{jr})} - l_{j1}\cos(\theta_j-\theta_{jr}) \tag{6}$$

Applying the sine law to the same triangle, substituting the value of θ_{jr} from (4), and solving for $\tilde{\theta}_j$, we obtain

$$\tilde{\theta}_j = \theta_j + \sin^{-1}\left(\frac{l_{j2}}{R_j}\sin(\sin^{-1}(\sqrt{\varepsilon}\sin\theta_j) - \theta_j)\right) \tag{7}$$

3.2 Computation of distances for determining propagation and focusing delays

In order to apply the synthetic aperture beamforming of (1)-(3) in the presence of a wall, we need to compute the distance from the transmitter to the point of interest $\tilde{\mathbf{x}}_\mathbf{j}$ and then back to the receiver along the refractive path. For propagation delays, $\tilde{\mathbf{x}}_\mathbf{j}$ represents the target location, whereas for computation of the focusing delays, $\tilde{\mathbf{x}}_\mathbf{j}$ corresponds to the pixel being imaged. The distance through the wall along the direction θ_{mji} is denoted by l_{mj1}, and l_{mj2} is the distance after refraction to the location $\tilde{\mathbf{x}}_\mathbf{j}$. From Fig. 3, it is easy to show that

$$l_{mj1} = \frac{d_w}{R_j\cos\theta_j} d(\mathbf{x_{tm}}, \mathbf{x_j}), \quad \cos\theta_{mji} = d_w / l_{mj1}, \quad \theta_{mjr} = \sin^{-1}(\sqrt{\varepsilon}\sin\theta_{mji}) \tag{8}$$

Using the cosine law to relate the distances $d(\mathbf{x_{tm}}, \mathbf{A})$, $d(\mathbf{A}, \tilde{\mathbf{x}}_\mathbf{j})$, and $d(\mathbf{x_{tm}}, \tilde{\mathbf{x}}_\mathbf{j})$, and solving for l_{mj2}, we obtain

$$l_{mj2} = \sqrt{(d(\mathbf{x_{tm}}, \tilde{\mathbf{x}}_\mathbf{j}))^2 - l_{mj1}^2 \sin^2(\theta_{mji} - \theta_{mjr})} - l_{mj1}\cos(\theta_{mji} - \theta_{mjr}) \tag{9}$$

Similarly, for propagation from $\tilde{\mathbf{x}}_\mathbf{j}$ to the n-th receiver at $\mathbf{x_{rn}}$ along the refractive path as shown in Fig. 4, we get

$$l_{nj1} = \frac{d_w}{R_j\cos\theta_j} d(\mathbf{x_{rn}}, \mathbf{x_j}), \quad \cos\theta_{njr} = d_w / l_{nj1}, \quad \theta_{nji} = \sin^{-1}(\sqrt{\varepsilon}\sin\theta_{njr}) \tag{10}$$

$$l_{nj2} = \sqrt{(d(\mathbf{x_{rn}}, \tilde{\mathbf{x}}_\mathbf{j}))^2 - l_{nj1}^2 \sin^2(\theta_{njr} - \theta_{nji})} - l_{nj1}\cos(\theta_{njr} - \theta_{nji}) \tag{11}$$

We are now in a position to present the wideband synthetic aperture beamformer for TWI. The following notation will be used. The position vector $\mathbf{x_j} = (R_j\sin\theta_j, R_j\cos\theta_j)$, where **j=p** (for target location) or **q** (for the pixel being imaged), represents the point towards which the signal is traveling through the wall. The point towards which the signal travels after refraction at the wall-air interface is denoted by $\tilde{\mathbf{x}}_\mathbf{j} = (R_j\sin\tilde{\theta}_j, R_j\cos\tilde{\theta}_j)$.

3.3 Design of the beamformer

Following the sequential transmission and reception approach described in Section 2 and after coherent combination of the delayed and weighted versions of the received signals, the complex amplitude image value for the pixel located at $\tilde{\mathbf{x}}_\mathbf{q} = (R_q\sin\tilde{\theta}_q, R_q\cos\tilde{\theta}_q)$, due to a single target located at $\tilde{\mathbf{x}}_\mathbf{p} = (R_p\sin\tilde{\theta}_p, R_p\cos\tilde{\theta}_p)$, is given by

$$I(\tilde{\mathbf{x}}_\mathbf{q}) = \sum_{m=1}^{M}\sum_{n=1}^{N} w_{tm}w_{rn}a(\tilde{\mathbf{x}}_\mathbf{p})\exp(-\alpha(l_{mp1} + l_{np1}))s(T - \tau_{mn} - \tilde{\tau}_{mn}) \tag{12}$$

where α is the attenuation constant of the wall. Incorporating the slowing of the waves due to propagation through the wall, the propagation delay τ_{mn} is given by

$$\tau_{mn} = \frac{l_{mp1}}{v} + \frac{l_{mp2}}{c} + \frac{l_{np1}}{v} + \frac{l_{np2}}{c}, \quad v = \frac{c}{\sqrt{\varepsilon}} \tag{13}$$

where l_{mp1} and l_{np1} are the distances traveled through the wall, and l_{mp2} and l_{np2} are the distances traveled beyond the wall, on transmit and receive and are given by (8), (10), (9) and (11) (with j=p) respectively. In (12), $\tilde{\tau}_{mn}$ is the focusing delay applied to the output of the n-th receiver when the transmitter is at the m-th location and is given by

$$\begin{aligned}\tilde{\tau}_{mn} = T - \frac{l_{mq1}}{v} - \frac{l_{mq2}}{c} - \frac{l_{nq1}}{v} - \frac{l_{nq2}}{c} &= T - \frac{1}{v}\frac{d_w}{R_q\cos\theta_q} d(\mathbf{x_{tm}}, \mathbf{x_q}) + \frac{1}{c}\frac{d_w}{R_q\cos\theta_q} d(\mathbf{x_{tm}}, \mathbf{x_q})\cos(\theta_{mqi} - \theta_{mqr}) \\ &- \frac{1}{c}\sqrt{(d(\mathbf{x_{tm}}, \tilde{\mathbf{x}}_\mathbf{q}))^2 - \frac{d_w^2}{R_q^2\cos^2\theta_q}(d(\mathbf{x_{tm}}, \mathbf{x_q}))^2\sin^2(\theta_{mqi} - \theta_{mqr})} - \frac{1}{v}\frac{d_w}{R_q\cos\theta_q} d(\mathbf{x_{rn}}, \mathbf{x_q}) \\ &- \frac{1}{c}\sqrt{(d(\mathbf{x_{rn}}, \tilde{\mathbf{x}}_\mathbf{q}))^2 - \frac{d_w^2}{R_q^2\cos^2\theta_q}(d(\mathbf{x_{rn}}, \mathbf{x_q}))^2\sin^2(\theta_{nqr} - \theta_{nqi})} + \frac{1}{c}\frac{d_w}{R_q\cos\theta_q} d(\mathbf{x_{rn}}, \mathbf{x_q})\cos(\theta_{nqr} - \theta_{nqi})\end{aligned} \tag{14}$$

Element #	1	2	3	4	5	6	7	8
Transmit (m)	-0.9	-0.3	0.3	0.6				
Receive (m)	-0.2625	-0.1875	-0.1125	-0.0375	0.0375	0.1125	0.1875	0.2625

Table 1: Transmit and Receive array locations

where θ_{mqi}, θ_{mqr}, θ_{nqi}, θ_{nqr} are given by (8) and (10) with $j=q$. The two-way time of flight, T, for the focusing point $\tilde{\mathbf{x}}_\mathbf{q}$ is obtained using (5) and (6) with $j=q$ and is given by

$$T = \frac{2l_{p1}}{v} + \frac{2l_{p2}}{c} = \frac{2}{v}\frac{d_w}{\cos\theta_q} + \frac{2}{c}\left(\sqrt{R_q^{\,2} - \frac{d_w^{\,2}}{\cos^2\theta_q}\sin^2(\theta_q - \theta_{qr})} - \frac{d_w}{\cos\theta_q}\cos(\theta_q - \theta_{qr})\right) \tag{15}$$

where θ_{qr} is given by (4) with $j=q$. The general case of multiple targets can be obtained by superposition.

3.4 Simulations

In this section, we present B-Scan (range vs. angle) images obtained using the beamformer of eq. (12). An amplitude modulated rectangular pulse of 1 GHz bandwidth centered at 2 GHz is used for imaging. The 4-element transmit and the 8-element receive array used are given in Table 1. The wall through which the system is looking is a 6" thick concrete wall with ε=9. The one-way attenuation through the wall is taken to be 6 dB for 6" thickness [8]. The room contains a stationary point target with a reflection coefficient of unity. In all figures, we plot the magnitude of the complex amplitude image, with maximum value normalized to unity.

Figures 5 and 6 present images of the target located at a range of 6 m and at an angle of 0° and 22° respectively. We can clearly see that in both the cases, the proposed beamformer has located the target position accurately.

4.0 ERROR ANALYSIS

Eq. (12) can be rewritten as

$$I(\tilde{\mathbf{x}}_\mathbf{q}) = \sum_{m=1}^{M}\sum_{n=1}^{N} w_{tm} w_{rn}\, r(T - \tilde{\tau}_{mn}) \tag{16}$$

where $r(t) = a(\tilde{\mathbf{x}}_\mathbf{p})\exp(-\alpha(l_{mp1} + l_{np1}))s(t - \tau_{mn})$ is the signal received at the n-th receiver when the m-th transmitter is used. Let $T_{mn} = T - \tilde{\tau}_{mn}$ be the modified focusing delay. Then,

$$I(\tilde{\mathbf{x}}_\mathbf{q}) = \sum_{m=1}^{M}\sum_{n=1}^{N} w_{tm} w_{rn}\, r(T_{mn}(\tilde{\mathbf{x}}_\mathbf{q})) \tag{17}$$

where the dependence of T_{mn} on $\tilde{\mathbf{x}}_\mathbf{q}$ is explicitly shown. Assume that the error in wall thickness is δ_w and that in the square root of ε is δ_ε. Then, the pixel value $\hat{I}(\tilde{\mathbf{x}}_\mathbf{q})$ is given by

$$\hat{I}(\tilde{\mathbf{x}}_\mathbf{q}) = \sum_{m=1}^{M}\sum_{n=1}^{N} w_{tm} w_{rn}\, r(\hat{T}_{mn}(\tilde{\mathbf{x}}_\mathbf{q})) \tag{18}$$

with $\hat{T}_{mn}$ given by

$$\begin{aligned}\hat{T}_{mn}(\tilde{\mathbf{x}}_\mathbf{q}) = {} & \frac{\sqrt{\varepsilon}+\delta_\varepsilon}{c}\frac{d_w+\delta_w}{R_q\cos\theta_q}d(\mathbf{x_{tm}},\mathbf{x_q}) + \frac{1}{c}\sqrt{(d(\mathbf{x_{tm}},\tilde{\mathbf{x}}_\mathbf{q}))^2 - \frac{(d_w+\delta_w)^2}{R_q^{\,2}\cos^2\theta_q}(d(\mathbf{x_{tm}},\mathbf{x_q}))^2\sin^2(\theta_{mqi}-\theta_{mqr})} \\ & - \frac{1}{c}\frac{d_w+\delta_w}{R_q\cos\theta_q}d(\mathbf{x_{tm}},\mathbf{x_q})\cos(\theta_{mqi}-\theta_{mqr}) + \frac{\sqrt{\varepsilon}+\delta_\varepsilon}{c}\frac{d_w+\delta_w}{R_q\cos\theta_q}d(\mathbf{x_{rn}},\mathbf{x_q}) \\ & + \frac{1}{c}\sqrt{(d(\mathbf{x_{rn}},\tilde{\mathbf{x}}_\mathbf{q}))^2 - \frac{(d_w+\delta_w)^2}{R_q^{\,2}\cos^2\theta_q}(d(\mathbf{x_{rn}},\mathbf{x_q}))^2\sin^2(\theta_{nqr}-\theta_{nqi})} - \frac{1}{c}\frac{d_w+\delta_w}{R_q\cos\theta_q}d(\mathbf{x_{rn}},\mathbf{x_q})\cos(\theta_{nqr}-\theta_{nqi})\end{aligned} \tag{19}$$

where θ_{mqi}, θ_{mqr}, θ_{nqi}, θ_{nqr} are given by (8) and (10) with $j=q$ and $\sqrt{\varepsilon}$ replaced by $\sqrt{\varepsilon}+\delta_\varepsilon$. It is clear from (19) that the errors in wall parameters manifest themselves as errors in focusing delays. As a result, the measured target location will not be equal to $\tilde{\mathbf{x}}_\mathbf{p}$. We are interested in finding the error introduced in the measured target location under these error conditions. The approach is to find $\tilde{\mathbf{x}}_\mathbf{q}$ at which the quantity

$\rho = \sum_m \sum_n (T_{mn}(\tilde{\mathbf{x}}_\mathbf{p}) - \hat{T}_{mn}(\tilde{\mathbf{x}}_\mathbf{q}))^2$ is a minimum, i.e., to find the pixel for which the corresponding set of focusing delays would optimally cancel the propagation delays, thereby identifying the new measured target location. Table 2 shows the solution, obtained numerically, optimal in the least squares sense under various error conditions for the imaging system of Section 3.4. The term E is ρ normalized by $(\sum_m \sum_n (T_{mn} - \hat{T}_{mn}))^2$. We observe that when there is error only in wall thickness, the magnitude of the error in measured target range is twice $|\delta_w|$. Also, when δ_w is positive, the target appears to be closer to the array and shifts closer to broadside, and vice versa. Figures 7 and 8 show the images computed using (18) for case 1 and case 4 of Table 2. Comparing the target location from these images to the predicted values of Table 2, we see that the least squares approach provides reasonably good results.

5.0 CONCLUDING REMARKS

We have presented a synthetic aperture beamformer whose hybrid "subarray-post data acquisition processing" design incorporates the effects of the wall, thereby rendering it suitable for through-the-wall imaging applications. Proof of concept is provided through simulation results. A least-squares performance measure has also been presented for the beamformer under conditions of errors in wall parameters for a single target scenario.

6.0 REFRENCES

[1] D. D. Ferris Jr. and N. C. Currie, "A survey of current technologies for through-the-wall surveillance (TWS)", *Proc. SPIE*, vol. 3577, pp. 62-72, Nov. 1998.

[2] R. T. Hoctor and S. A. Kassam, "The unifying role of the coarray in aperture synthesis for coherent and incoherent imaging", *Proc. IEEE*, vol. 78, no. 4, pp. 735-752, Apr. 1990.

[3] F. Ahmad and S. A. Kassam, "Coarray analysis of the wide-band point spread function for active array imaging" *Signal Processing*, vol. 81, pp. 99-115, Jan 2001.

[4] A. K. Luthra, S. A. Kassam, and R. B. Bernardi, "Body imaging using vectorial addition of acoustic reflection to achieve effect of scanning beam continuously focused in range", U.S. Patent No. 4,604,697, 1986.

[5] R. T. Hoctor and S. A. Kassam, "Array redundancy for active line arrays", *IEEE Trans. on Image Processing*, vol. 5, no. 7, pp. 1179-1183, 1996.

[6] F. Ahmad, et. al., "Aperture synthesis for a through-the-wall imaging system", *Proc. ISSPIT*, Dec. 2002.

[7] R. Benjamin, et. al., "Through-wall imaging using real-aperture radar", *Proc.URSI General Assembly*, Aug., 2002.

[8] L. M. Frazier, "Radar Surveillance through Solid Materials" , *Proc. SPIE.*, vol. 2938 , pp. 139-146, Nov. 1996.

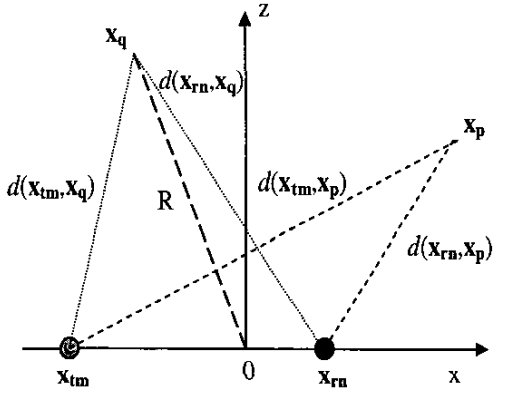

Figure 1: Geometry of the scene being imaged

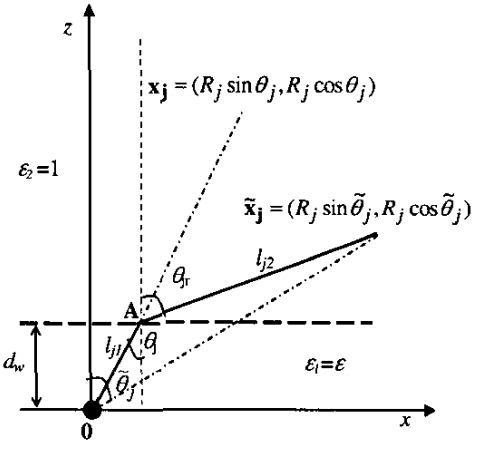

Figure 2: Geometry depicting refraction

R_p (m)	$\tilde{\theta}_p$ (°)	δ_w (m)	δ_ε	R_q (m)	$\tilde{\theta}_q$ (°)	E
6.0	0	0.02	0	5.9695	0	0.4044
6.0	0	-0.02	0	6.0507	0	0.3991
6.0	22	0.02	0	5.9685	21.8077	0.0436
6.0	22	-0.02	0	6.0517	22.1855	0.0412
6.0	22	-0.02	0.25	6.0158	21.8026	0.0496

Table 2: Least-squares solution corresponding to various erroneous conditions

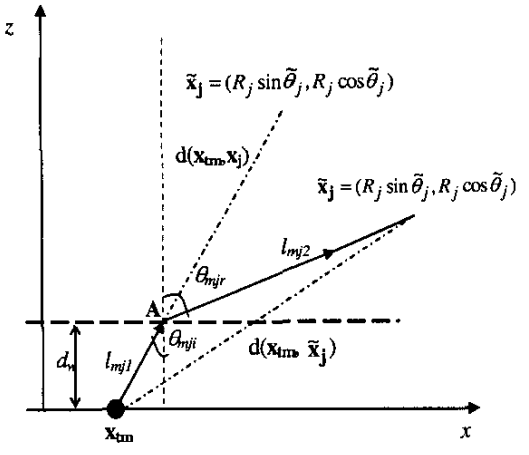

Figure 3: Geometry for computing distances on transmit

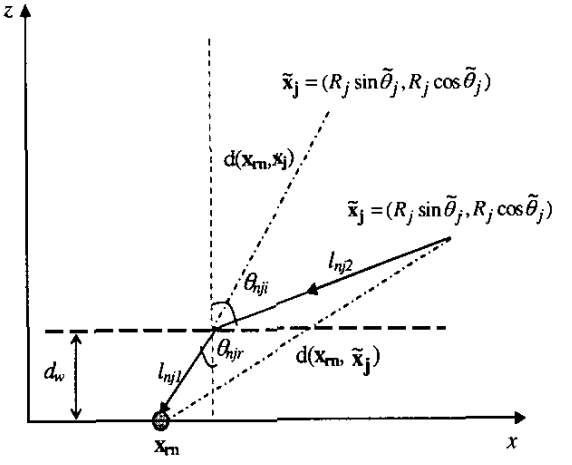

Figure 4: Geometry for computing distances on receive

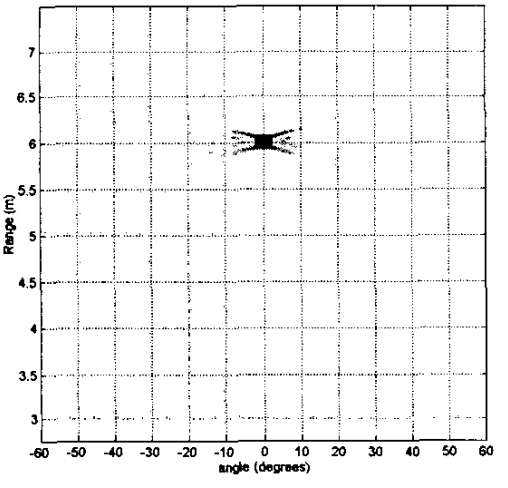

Figure 5: Image of target at 6 m and at an angle of 0°

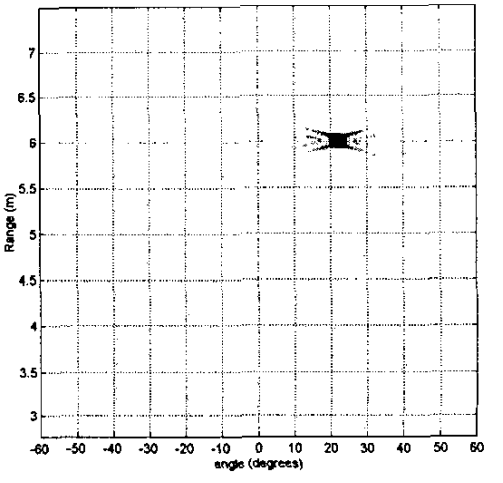

Figure 6: Image of target at 6 m and at angle 22°

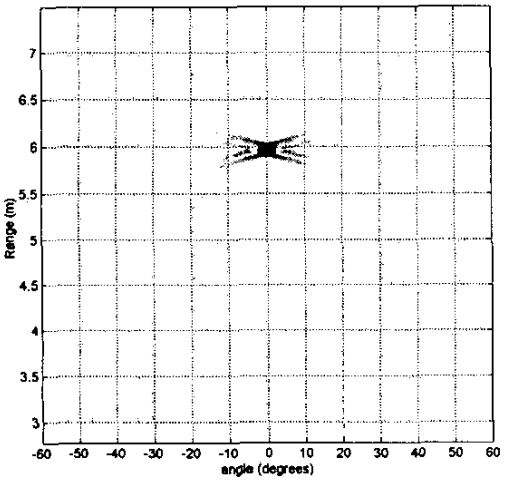

Figure 7: Image of target located at (6.0m, 0°)

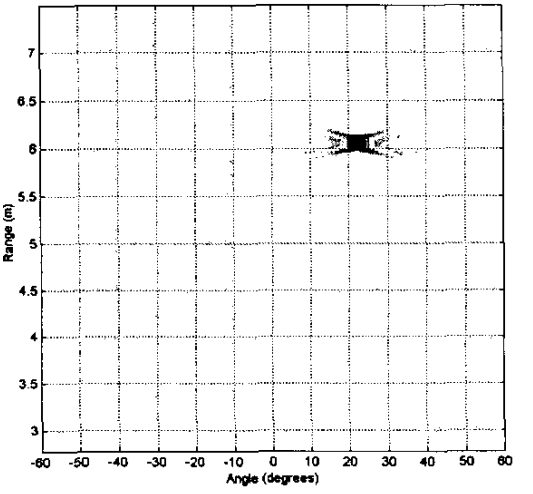

Figure 8: Image of target located at (6.0m, 22°)